COHERENCE

The concept of coherence, when applied to wave phenomena, implies a well-defined relationship in phase and frequency for the propagation of a wave or group of waves: the various components of the wavepacket are well organized, and their cohesion is maintained over large distances and times. Coherence distinguishes such phenomena from random noise signals, regardless of intensity or power level. The relevance of this fun-

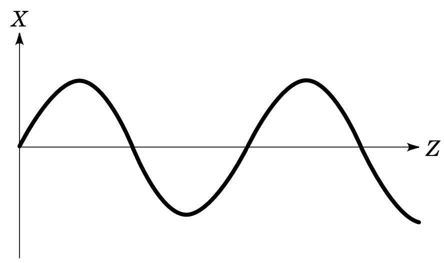

Figure 1. Monochromatic plane wave.

damental concept extends to many different types of waves, including pressure waves (sound), electromagnetic waves (light), quantum wavepackets (atoms and elementary particles), and gravitational waves.

In the case of electromagnetic waves, comparing a laser beam with an incoherent light source such as a flashlight qualitatively illustrates the fundamental features of coherence, as revealed by basic experiments. In particular, a laser beam readily produces interference patterns, thus exhibiting spatial coherence, and the intense, monochromatic character of laser light is an indication of its temporal coherence. The propagation of laser light in the form of a Gaussian, diffraction-limited beam, as shown by its capacity to be focused extremely tightly, demonstrates transverse spatial coherence.

The basic concept of coherence is illustrated in Figs. 1 and 2, where monochromatic (single-frequency) plane waves are first considered. A simple mathematical description of such a

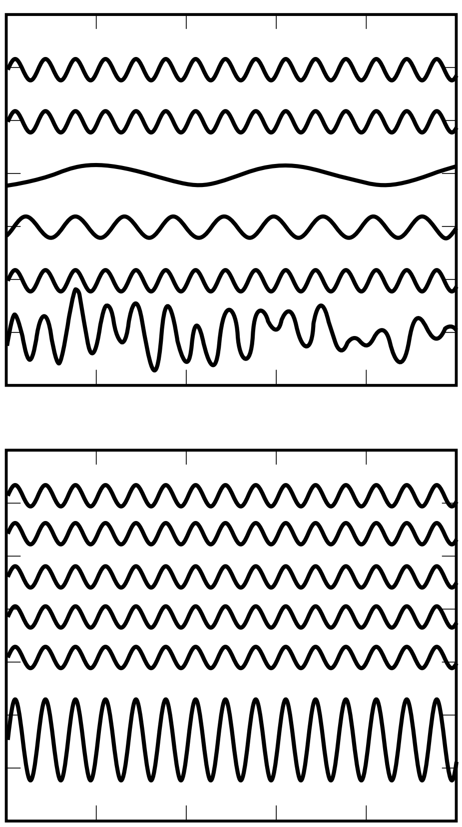

Figure 2. (Top) Incoherent superposition of plane waves. (Bottom) Coherent superposition of monochromatic plane waves.

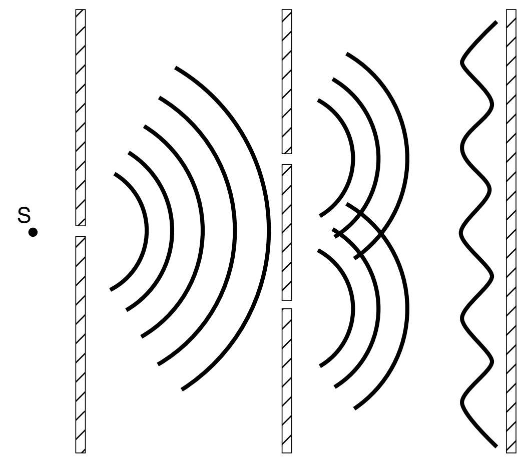

Figure 3. Schematic of Young's double-slit experiment.

harmonic plane wave can be given in terms of the associated field,

$$\mathbf{E}(\mathbf{x}, t) = \hat{x}E \sin[\phi(\mathbf{x}, t)]$$

where the quantity

$$\phi(x, t) = \omega t - \mathbf{k} \cdot \mathbf{x} + \phi_0 = \omega t - kz + \phi_0$$

is the phase of the wave, while E represents its amplitude, and $\hat{x}$ corresponds to its polarization state (linear, in this case). The sine function describes the harmonic variation of the wave with space and time. The parameter ω is the frequency of the wave, and $\mathbf{k}$ is its wavenumber, which defines both the wavelength and the direction of propagation (chosen here in the direction of positive z, with $\mathbf{k} = \hat{z}k$). As dispersion and coherence are two very closely interrelated concepts, the important relation between frequency and wavenumber will be discussed in some detail in subsequent paragraphs.

To study the overall effect of the waves shown in Fig. 2, the principle of superposition is applied, which simply states that the resultant wave is obtained by summing vectorially over the fields of the incident waves. In the first case (top), the waves are phased randomly, and they interfere destructively to produce a low amplitude field, characteristic of an incoherent process. By contrast, in the second case (bottom), the waves have the same phase and add up coherently. The intensity of the resulting wave is obtained by taking the square of the field, and it is easily seen that in the case of the superposition of N waves of equal amplitudes, the coherent intensity scales as N^2, while the incoherent radiation intensity only increases linearly with N. Finally, it should be noted that the principle of superposition holds for linear waves only, such as electromagnetic radiation in a vacuum (below the Schwinger critical field, where spontaneous pair creation occurs), or quantum-mechanical probability waves. In the case of nonlinear media, coherence takes a more subtle form, yielding a rich variety of complex phenomena.

It is interesting to note that in some cases, as illustrated in Fig. 3 by the famous double-slit experiment, an incoherent point source can be utilized to produce interference patterns due to spatial coherence only. This can be readily understood by noting that in this type of configuration, a single wavepacket is made to self-interfere at a given time, thus eliminating temporal coherence considerations. The quantum mechanical version of this experiment applies equally well to photons (electromagnetic waves) or electrons (probability wavefunctions), and the self-interference aspect of the process clearly illustrates the quantum wave-particle duality.

The earliest scientific observations of coherence were made by Christiaan Huygens (1629–1695), Sir Isaac Newton (1642–1727), and Augustin Jean Fresnel (1788–1827), who considered interference effects at optical wavelengths. In particular, diffraction patterns and interference fringes were studied in detail and led to the wave theory of light, which was subsequently identified with electromagnetic radiation through the fundamental work of James Clerk Maxwell (1831–1879). Powerful mathematical concepts, including sine and cosine transforms, were introduced by Joseph Fourier (1768–1830) and other mathematicians to study the physics of waves, including their propagation, diffraction, and interference.

Until the early twentieth century, wave experiments were essentially limited to the visible part of the electromagnetic spectrum, although sound waves, which can exhibit coherence, were also studied. Coherent radiation sources now cover the electromagnetic spectrum from ultra-low frequency (ULF) waves used for underwater communications, through millimeter-waves, and the far infrared (FIR) and infrared (IR) regions of the spectrum, to the vacuum ultraviolet (VUV). Free-electron devices, including microwave tubes and free-electron lasers (FELs), cover most of this range, while atomic lasers are predominant in the IR-UV range. A free-electron laser extracts electromagnetic energy from a relativistic electron beam through resonant interaction with a fast electromagnetic wave ($v_\phi > c$). Atomic X-ray lasers have also been developed using radiative and cascade recombination schemes.

Quantum mechanics introduced a new type of wave with the early work of Louis de Broglie, Niels Bohr, Erwin Schroedinger, and Werner Heisenberg, who postulated the existence of matter waves, later identified with a state vector Ψ governed by the Schroedinger equation. This wavefunction was physically interpreted in terms of a probability density $\Psi\Psi^*$ by Max Born. In the context of quantum mechanics, atomic levels can be viewed as the stable interference of electron wavefunctions in the Coulomb field of the nucleus. The experiments of Clinton Joseph Davisson and Lester Halbert Germer (1) first demonstrated the diffraction of electron waves by a nickel crystal.

Recently, remarkable experiments using Bose-Einstein condensates to generate coherent atomic beams have been performed at MIT (2), where the coherence of the condensate wavefunction was verified by measuring its interference with a second atomic beam. The question of quantum decoherence, also referred to as "wavefunction collapse," is one of the current outstanding problems in modern physics, as exemplified by the ubiquitous "Schroedinger's cat" paradox. Finally, with the generalization of quantum field theories (3) to describe the strong and electroweak interactions, in terms of fermionic (charges) and bosonic (interaction carriers) fields, coherence and interference are now conspicuous throughout modern physics.

In terms of applications, the concept of coherence is also very pervasive in advanced technologies, ranging from masers and lasers, spectroscopy, imaging, holography, and Doppler radars, to stellar interferometry, UV and X-ray microlithography, microwave sources, free-electron lasers, particle accelerators, plasma physics, as well as advanced biomedical techniques.

This article is organized as follows. After a brief discussion of dispersion, the radiation characteristics of free electrons are described in some detail, within the framework of classical electrodynamics (CED). For point charges, the radiation is always coherent because no cutoff is introduced. For extended charge distributions, however, there is a physical scale that sets the transition from coherent to incoherent radiation; this mechanism is discussed, as well as spatial coherence (transverse modes), phase noise in free-electron devices, nonlinear coherent scattering processes (Compton, Kapitza-Dirac, ponderomotive), and radiative corrections. Next, the coupling of bound electrons to electromagnetic fields in quantum systems, as exemplified by the atomic laser, is reviewed, together with recent major advances in this field, including chirped pulse amplification (CPA), temporal shaping and imaging, and femtosecond (10^{-15} s) optics. A "chirped" pulse is characterized by a frequency that has temporal dependence.

The important question of whether coherence implies or requires monochromaticity is also addressed. In a classic paper (4), Roy J. Glauber introduced higher-order correlation functions, and demonstrated that coherent fields can be generated with arbitrary Fourier spectra. This formalism is presented in detail in a monograph (5) by Leonard Mendel and Emil Wolf and will be summarized here. Finally, other topics in quantum optics and laser-plasma interaction physics, related to the general concept of coherence, are briefly discussed, including nonlinear processes, phase conjugation, *squeezed* states, four-wave mixing, and decoherence.

COHERENCE IN FREE-ELECTRON DEVICES

Dispersion

The aforementioned relation between the frequency and wavenumber is called the dispersion equation and contains important information about the propagation of waves in a particular medium. For example, in the case of electromagnetic waves propagating in a vacuum, $\omega^2/c^2 - \mathbf{k}^2 = 0$, with solutions $k = \pm\omega/c$. In this case, the two solutions for the wavenumber are linear functions of the frequency, which indicate that the vacuum is a nondispersive medium. In general, expressing the wavenumber as a function of frequency yields a complex, nonlinear set of solutions. Each particular solution represents a mode of propagation. In the case where the propagation of a pulse is studied, the wavepacket can be Fourier-transformed into the frequency domain, yielding a spectrum centered at a given frequency, ω_0. The nonlinearities of the dispersion can now be Taylor-expanded around that central frequency to first yield the central wavelength of the pulse,

$$\lambda_0 = \frac{2\pi}{k(\omega_0)}$$

then the corresponding group velocity,

$$\frac{\partial k}{\partial \omega}(\omega_0) = \frac{1}{v_g(\omega_0)}$$

which gives the propagation velocity of the center of the pulse, while the quadratic term in the expansion

$$\frac{\partial^2 k}{\partial \omega^2}(\omega_0) = \frac{-1}{v_g^2(\omega_0)} \frac{\partial v_g}{\partial \omega}(\omega_0)$$

is related to group velocity dispersion (GVD). Higher-order terms in the expansion describe more complex distortions of the pulse as it propagates through the medium under consideration.

In addition, the dispersion relation can often take a tensorial form, as in the case of anisotropic media, and its complex characteristics (imaginary part of the wavenumber) indicate attenuation or amplification of the waves in the medium. Finally, the relation between the frequency and wavenumber can also depend on the intensity of the wave. In this case, the medium is called nonlinear, and the propagation of waves in such a system can yield a very rich variety of phenomena, ranging from self-focusing and self-phase modulation to soliton propagation and harmonic generation. The dispersion characteristics of a medium are often given in terms of its refractive index,

$$n(\omega) = \frac{ck(\omega)}{\omega} = \frac{c}{v_\phi(\omega)} = c\sqrt{\epsilon(\omega)\mu(\omega)}$$

which scales like the inverse of the phase velocity and can also be related to the relative electric permittivity and magnetic permeability of the material. These tensors indicate how the external, or incident, electromagnetic fields induce both charge and current densities as they propagate through the medium, thus giving rise to complex, nonlinear inductions, which, in turn, modify the propagation of the wave.

Boundary conditions, such as those imposed by a waveguide structure or an optical resonator, also modify the dispersion characteristics of an electrodynamic system. Typically, those boundaries introduce a quantization of the transverse mode spectrum, characterized by a discrete cutoff frequency spectrum. In a resonator, the axial modes also form a discrete spectrum. In both cases, any space- and time-dependent electromagnetic field configuration can be described as a superposition of such modes, as they form a complete system of eigenfunctions for the system under consideration. The corresponding eigenvalue spectra describe the dispersion properties of each mode. The combination of a Fourier transform for the time-dependent part of the wave, together with a transverse eigenmode series expansion, is a powerful mathematical tool to analyze wave propagation and coherence in detail. This technique will now be fully illustrated.

Radiation Characteristics of a Point Charge

A simple approach to the description of coherent radiation processes can be constructed within the framework of classical electrodynamics and help illustrate the concept of coherence. For completeness, a brief review of the most important ideas of radiation theory is first given.

The interaction of charged particles with electromagnetic fields can be described, in the classical limit, by two sets of equations. On the one hand, there are Maxwell's two groups of equations, governing the fields

$$\nabla \times \mathbf{E} + \partial_t \mathbf{B} = 0 \tag{1}$$

$$\nabla \cdot \mathbf{B} = 0 \tag{2}$$

and the group with sources

$$\nabla \cdot \mathbf{E} = \frac{1}{\epsilon_0}\rho \tag{3}$$

$$\nabla \times \mathbf{B} - \frac{1}{c^2}\partial_t \mathbf{E} = \mu_0 \mathbf{j} \tag{4}$$

On the other hand, there are the equations governing the particles' dynamics, which are given by the expression of the Lorentz force,

$$d_t \mathbf{p} = -e(\mathbf{E} + \mathbf{v} \times \mathbf{B}) \tag{5}$$

and the continuity equation, which corresponds to charge or particle conservation,

$$\partial_t \rho + \nabla \cdot \mathbf{j} = 0 \tag{6}$$

Here, $j_\mu \equiv (c\rho, \mathbf{j}) = -enc(1, \boldsymbol{\beta})$ is the four-vector current density, with n the particle density, and $\mathbf{v} = c\boldsymbol{\beta}$ their velocity. The particles' momentum is given by $\mathbf{p} = m_0 c\mathbf{u}$, and their energy is given by $m_0c^2\gamma$, where we have introduced the four-velocity $u_\mu \equiv (\gamma, \mathbf{u}) = \gamma(1, \boldsymbol{\beta})$. In this notation, the four-velocity corresponds directly to the normalized energy-momentum: $p_\mu \equiv (\xi/c, \mathbf{p}) = m_0 c u_\mu$, with ξ the energy. At this point, it is important to note that Maxwell's source-free Eqs. (1) and (2) suggest the introduction of the four-vector potential $A_\mu \equiv (\phi/c, \mathbf{A})$, defined such that

$$\mathbf{E} = -\nabla\phi - \partial_t \mathbf{A} \tag{7}$$

$$\mathbf{B} = \nabla \times \mathbf{A} \tag{8}$$

As a result, Eqs. (1) and (2) are automatically satisfied. If, in addition, we impose that the four-vector potential satisfies the Lorentz gauge condition

$$\frac{1}{c^2}\partial_t \phi + \nabla \cdot \mathbf{A} = 0 \tag{9}$$

we see that the second group is equivalent to

$$\left[\nabla^2 - \frac{1}{c^2}\partial_t\right]\phi + \frac{1}{\epsilon_0}\rho = 0 \tag{10}$$

$$\left[\nabla^2 - \frac{1}{c^2}\partial_t\right]\mathbf{A} + \mu_0 \mathbf{j} = 0 \tag{11}$$

Equations (10) and (11) can be conveniently grouped in a single covariant wave equation (6),

$$\left[\nabla^2 - \frac{1}{c^2}\partial_t^2\right]A_\mu + \mu_0 j_\mu = [\partial_\nu \partial^\nu]A_\mu + \mu_0 j_\mu = 0 \tag{12}$$

where the four-gradient operator is defined by

$$\partial_\mu \equiv \frac{\partial}{\partial x^\mu} \equiv -\left(\frac{1}{c}\partial_t, \nabla\right)$$

In this form, the gauge equation and the Lorentz force equation simply read

$$\partial_\mu A^\mu = 0 \tag{13}$$

$$d_\tau u_\mu = -e(\partial_\mu A_\nu - \partial_\nu A_\mu)u^\nu \tag{14}$$

The covariant notation used here corresponds to a flat hyperbolic metric, where the scalar product is defined as $a_\mu b^\mu = \mathbf{a} \cdot \mathbf{b} - a_0 b_0$, with the subscript 0 referring to the temporal component of a four-vector, while the bold characters correspond to the usual spatial three-vectors (6). For example, we have $u_\mu u^\mu = (\gamma\boldsymbol{\beta})^2 - \gamma^2 = \gamma^2(\boldsymbol{\beta}^2 - 1) = -1$. The proper time is defined by $dt/d\tau = \gamma$, and the four-velocity can now be defined in terms of the position: $u_\mu = dx_\mu/d\tau$.

Note that the four-vector potential can be modified according to

$$\mathbf{A} \rightarrow \mathbf{A} + \nabla\Lambda, \quad \phi \rightarrow \phi - \partial_t \Lambda, \quad A_\mu \rightarrow A_\mu + \partial_\mu \Lambda \tag{15}$$

while the fields remain unchanged. Here, Λ is an arbitrary function of space and time. The invariance of the fields under such a transform is called gauge invariance. This concept, together with covariance (invariance under Lorentz transformations), entirely specifies classical and quantum electrodynamics (QED).

The driven wave Eq. (12) is linear, and the principle of superposition applies to its solutions. In particular, if a solution to the wave equation is known for a Dirac delta-function source, it can be immediately generalized, as any four-current density source can be appropriately described by an integral superposition of delta-functions:

$$\mathbf{j}_\mu(x_\nu) = \int\int\int\int \mathbf{j}_\mu(x'_\nu)\delta_4(x_\nu - x'_\nu)\, d^4 x_\nu \tag{16}$$

The general radiation problem then takes the form

$$[\partial_\nu \partial^\nu] G(x_\nu - x'_\nu) + \mu_0 \delta_4(x_\nu - x'_\nu) = 0 \tag{17}$$

The solution to this problem, G, known as the Green function of the problem, is therefore of particular importance. The details of the resolution fall out of the scope of this article, and can be found in the classic monographs by Pauli (6) and Jackson (7), for example. The main steps of the derivation involve Fourier-transforming the driven wave equation into momentum space, where $\partial_\mu \rightarrow ik_\mu$, and using a complex contour integral to avoid the poles corresponding to the vacuum dispersion on the past and future light-cones. There are two distinct solutions corresponding to retarded and advanced waves propagating at c in a vacuum in the absence of any structure:

$$G^\pm = -\left(1 \pm \frac{x_0 - x'_0}{|x_0 - x'_0|}\right)\delta(s^2) \tag{18}$$

where $s^2 = (x - x')_\mu (x - x')^\mu$ is the space-time interval, and $(x_0 - x'_0)$ is the time-like separation.

It is also important to note that the radiation of a point charge in arbitrary motion can be described in terms of Green functions (6,7) by expressing its four-current density as

$$\mathbf{j}_\mu(x_\nu) = ec\frac{u_\mu}{\gamma}(x_\nu)\delta_3(\mathbf{x}) = ec\int_{-\infty}^{\infty} u_\mu(x'_\nu)\delta_4(x_\nu - x'_\nu)\, d\tau' \tag{19}$$

where the charge density of the particle is modeled by a three-dimensional delta-function that has been generalized to four dimensions by integrating over the electron's proper time. The four-vector $u_\mu/\gamma \equiv (1, \boldsymbol{\beta})$ corresponds to the particle's three-velocity.

The four-vector potential corresponding to the retarded (causal) Green function is called the Lienhard-Wiechert potential, and has the covariant form

$$A_\mu(x_\nu) - \frac{1}{c}\phi(x_\nu)\frac{u_\mu}{\gamma}, \quad \phi(x_\nu) = \frac{1}{4\pi\epsilon_0}\frac{e}{R(1 - \boldsymbol{\beta}\cdot\hat{n})} \tag{20}$$

where all the dynamical quantities are evaluated at the retarded time, defined such that

$$R = c(t - t^-) = |\mathbf{x} - \mathbf{r}(t^-)| \tag{21}$$

and accounting for the propagation delay. Here, $x_\nu \equiv (ct, \mathbf{x})$ corresponds to the observation position and time, while $\mathbf{r}(t)$ describes the trajectory of the source (in particular, $\boldsymbol{\beta} = d\mathbf{r}/dt$), and $\hat{n}$ is the unit vector from the retarded position to the point of observation.

The corresponding electric and magnetic fields are derived using Eqs. (7) and (8), with the result that

$$\begin{aligned} \mathbf{E}(\mathbf{x}, t) &= \frac{e}{4\pi\epsilon_0}\left[\frac{\hat{n} - \boldsymbol{\beta}}{\gamma^2(1 - \boldsymbol{\beta}\cdot\hat{n})^3 R^2} + \frac{\hat{n}\times(\hat{n} - \boldsymbol{\beta})\times\dot{\boldsymbol{\beta}}}{(1 - \boldsymbol{\beta}\cdot\hat{n})^3 Rc}\right]_{t=t^-} \\ \mathbf{B}(\mathbf{x}, t) &= \hat{n}\times\frac{\mathbf{E}(\mathbf{x}, t)}{c} \end{aligned} \tag{22}$$

where the first term in the brackets essentially corresponds to the Lorentz transform of the Coulomb field (also called "velocity field"), while the second term, which carries energy to infinity, is the radiation (or "acceleration") field. The radiated power flux is given by the Poynting vector:

$$\mathbf{S} = \hat{n}\frac{dP}{R^2\, d\Omega} = \mathbf{E}\times\mathbf{H} = \hat{n}\frac{\mathbf{E}^2}{\mu_0 c} \tag{23}$$

The power scales like the square of the field and acceleration. It is easily seen that, in the instantaneous rest frame of the electron ($\boldsymbol{\beta} = \mathbf{0}$), the radiation pattern is always dipolar:

$$\mathbf{S} = \hat{n}\frac{e^2}{16\pi^2\epsilon_0 c}\frac{\dot{\boldsymbol{\beta}}^2\sin^2\xi}{R^2} \tag{24}$$

with the typical $\sin^2$ angular dependence. Here, ξ is the angle between the acceleration and the direction of observation. In any other frame, the relativistic Doppler effect warps this pattern and strongly favors forward scattering. The total radiated power is obtained by integrating the Poynting vector flux $R^2(\mathbf{S}\cdot\hat{n})$ over all solid angles, while the radiated momentum is given by the integral of $R^2\mathbf{S}$ over the same domain. In covariant form, this yields

$$\frac{dG_\mu}{d\tau} = \frac{\mu_0 e^2}{6\pi}(a_\nu a^\nu)u_\mu \tag{25}$$

where G_μ is the radiated energy-momentum, and $a_\mu = du_\mu/d\tau$ is the four-acceleration of the source. Finally, the radiated spectral energy density can be derived by Fourier-transforming the source trajectory and using Parsival's Theorem (7) to obtain

$$\frac{d^2I(\omega,\hat{n})}{d\omega\, d\Omega} = \frac{e^2\omega^2}{16\pi^3\epsilon_0 c}\left|\int_{-\infty}^{\infty} \hat{n}\times(\hat{n}\times\boldsymbol{\beta}\exp\left[i\omega\left(t-\frac{\hat{n}\cdot\mathbf{r}(t)c}{c}\right)\right]\, dt\right|^2 \tag{26}$$

Note that the question of coherence does not appear explicitly in this picture, as the point source has no physical scale, and radiates coherently at any wavelength. To complete this brief overview of classical electrodynamics, it is worth mentioning the question of radiative effects: as shown in Eq. (25), the electromagnetic field radiated by the accelerated source carries both energy and momentum; therefore, one should expect the particle to recoil as it radiates. For a point charge, this effect is essentially a self-interaction and has been derived by Dirac (8) in 1938. The lowest-order correction yields the Dirac-Lorentz equation

$$\begin{aligned} a_\mu &= -e(\partial_\mu A_\nu - \partial_\nu A_\mu)u^\nu + \tau_0\left[\frac{da_\mu}{d\tau} - (a_\nu a^\nu)u_\mu\right] \\ &= -eF_{\mu\nu}u^\nu + \tau_0\left[\frac{da_\mu}{dt} - G_\mu\right] \end{aligned} \tag{27}$$

where we recognize the usual Lorentz force and the negative of the radiated energy-momentum, which is identified with the radiation damping force. The supplementary term, which corresponds to the third-order derivative of the particle position, is required to satisfy the condition

$$u_\mu a^\mu = \frac{1}{2}\frac{d}{d\tau}(u_\mu u^\mu) = 0$$

and is called the Schott term. The parameter

$$\tau_0 = \frac{2}{3}\frac{r_0}{c} = 6.26\times 10^{-24}\ \mathrm{s}$$

is the Compton time-scale, where r_0 is the classical electron radius. This scale is the only natural scale appearing in classical electrodynamics, and it is interesting to note that the ratio of the Compton wavelength of the electron to its classical radius,

$$\frac{\lambda_c}{r_0} = \frac{1}{\alpha} = 137.036$$

is the inverse of the fine structure constant. Therefore, QED effects generally become important before radiative recoil strongly modifies the electron dynamics.

Coherent Synchrotron Radiation

The question of coherence in free-electron devices can now be addressed by considering the radiation characteristics of an accelerated charge distribution. The transition from coherent to incoherent radiation is modeled by considering the ratio of the electron bunch length to the radiation wavelength. The spatial coherence corresponds to the excitation of transverse modes in the system, and phase noise can be analyzed by considering the dispersion characteristics of the structure. For the sake of illustration, a fairly specific example is considered: coherent synchrotron radiation in a cylindrical waveguide FEL structure. The ideas presented here are easily generalized to other free-electron devices. In the presence of a helically polarized magnetic field, monoenergetic electrons can be launched on helical trajectories (9),

$$\boldsymbol{\beta}(r,\theta,z,t) = \hat{z}\beta_\parallel + \beta_\perp[\hat{r}\cos(k_w z-\theta) + \hat{\theta}\sin(k_w z - \theta)] \tag{28}$$

where the perpendicular velocity is given in terms of the wiggler field amplitude B_w, wavenumber k_w, and initial energy γ_0, by

$$\beta_\perp = \frac{eB_w}{\gamma_0 m_0 k_w c}$$

and where energy conservation yields

$$\frac{1}{\gamma_0^2} = 1 - \beta_\parallel^2 - \beta_\perp^2$$

The axially extended electron bunch charge density is described by a Gaussian distribution moving along the z axis with the axial velocity $\beta_\parallel c$

$$\rho(r,z,t) = \frac{q}{\sqrt{\pi}\,\Delta z\,\pi r_\perp^2}\exp\left[-\frac{(z-\beta_\parallel ct)^2}{\Delta z^2}\right] \quad r\le r_\perp \tag{29}$$

where q is the total bunch charge, Δz its characteristic axial scale length, and $r_\perp$ its radius. The corresponding current density in the helically polarized wiggler is then given by

$$\mathbf{j}(\theta,z,t) = \hat{z}\beta_\parallel c\rho(z,t) + \beta_\perp c\rho(z,t)[\hat{r}\cos(k_w z-\theta) + \hat{\theta}\sin(k_w z-\theta)] \tag{30}$$

To solve the driven wave equation in this case, it is useful to start by deriving the temporal Fourier transform of the current density. We have, by definition,

$$j_r(r,\theta,z,t) = \frac{1}{\sqrt{2\pi}}\int_{-\infty}^{\infty} d\omega\,\tilde{j}_r(r,\theta,z,\omega)\exp(-i\omega t) \tag{31}$$

where the Fourier transform is given by

$$\tilde{j}_r(\theta,\omega,z) = \frac{q\beta_w}{\sqrt{2}\pi^{3/2}r_\perp^2}\cos(k_w z-\theta)\exp\left(i\frac{\omega z}{\beta_\parallel c}\right)\exp\left[-\left(\frac{\omega\,\Delta z}{2\beta_\parallel c}\right)^2\right] \tag{32}$$

The Gaussian function corresponds to the coherence factor: for charge density distributions that are very short compared to the radiation wavelength, $\omega\Delta z \ll 1$, and the Gaussian is very close to unity; for arbitrarily short wavelength radiation, the coherence factor vanishes exponentially.

The dispersive characteristic of the structure can now be derived using a transverse eigenmode expansion. Note that these transverse modes, which satisfy the boundary conditions of the waveguide FEL, are spatially coherent. The degree of mixing of the transverse modes is a direct measurement of the transverse spatial coherence of the radiation generated in the FEL.

The transverse wave equation, for cylindrical geometry, is

$$\left(\Delta - \frac{1}{c^2}\partial_t^2\right)A_r - \frac{1}{r^2}(A_r + 2\partial_\theta A_\theta) = \mu_0 j_r \tag{33}$$

It is easily seen that in the case of a spatially extended charge distribution propagating in a helical wiggler, the transverse electric (TE) modes couple to the wiggler-induced motion, while the transverse magnetic (TM) modes are driven by the uniform motion of the space-charge distribution in the cylindrical waveguide. Only the TE modes are considered here.

The general method of resolution for this very general class of electrodynamical problem consists in separating variables and expanding the transverse components of the four-vector potential in terms of transverse vacuum eigenmodes of the structure, satisfying the appropriate boundary conditions. In the example treated here, the radial and azimuthal components of the four-vector are expanded in terms of the TE cylindrical eigenmodes and Fourier-transformed into frequency space, which yields the following expressions:

$$A_r(r,\theta,z,t) = \frac{1}{\sqrt{2\pi}} \sum_m \sum_n \int_{-\infty}^{+\infty} d\omega \tilde{A}_{mn}(z,\omega) \times \frac{J_m(\chi'_{mn} r/a)}{\chi'_{mn} r/a} \exp[i(m\theta - \omega t)] \tag{34}$$

$$A_\theta(r,\theta,z,t) = \frac{1}{\sqrt{2\pi}} \sum_m \sum_n \int_{-\infty}^{+\infty} d\omega \tilde{A}_{mn}(z,\omega) \times \frac{i}{m} J'_m(\chi'_{mn} r/a) \exp[i(m\theta - \omega t)] \tag{35}$$

Here, χ'_{mn} is the nth zero of the Bessel function derivative J'_m, and a is the waveguide radius. The explicit dependence on the axial coordinate z is retained to obtain a differential equation governing the spectral density of each TE mode. It is important to note here that, in very general terms, there is a one-to-one correspondence between the geometry of the electrodynamical system under consideration and the mathematical structure of the eigenmodes. For each boundary condition for a given spatial coordinate, a discrete eigenmode results: for instance, in the present case, the radial boundary conditions yield a discrete spectrum of Bessel functions, while the azimuthal symmetry results in a discrete set of harmonic functions in the angular coordinate θ. For unbounded variables, such as time, a continuous spectrum emerges; in the present case, it is represented by a Fourier transform into frequency space. Inserting these expressions into the driven wave equation, expressed in frequency space after Fourier-transforming the current density [see Eq. (32)], one obtains

$$\sum_m \sum_n \left(\frac{\omega^2}{c^2} - \frac{\chi'^2_{mn}}{a^2} + \partial_z^2 \right) \tilde{A}_{mn}(\omega,z) \frac{J_m(\chi'_{mn} r/a)}{\chi'_{mn} r/a} e^{im\theta} = \frac{\mu_0 q \beta_w}{\sqrt{2}\pi^{3/2} r_\perp^2} \cos(k_w z - \theta) \exp\left(-i\frac{\omega z}{\beta_\parallel c}\right) \exp\left[-\left(\frac{\omega\,\Delta z}{2\beta_\parallel c}\right)^2\right] \tag{36}$$

The next important step in the derivation is to use the orthogonality of the transverse eigenmodes to diagonalize this infinite set of coupled differential equations. This is achieved by applying the following operator

$$\int_0^{2\pi} d\theta e^{ip\theta} \int_0^{\mathrm{a}} r^2\, dr\, J_p\left(\frac{\chi'_{pq} r}{a}\right) \tag{37}$$

to Eq. (36). The operator introduced above diagonalizes the left-hand side of Eq. (36), while it projects the source term on a particular TE_{pq} cylindrical waveguide mode. This technique is rigorously analogous to the eigenfunction analysis used to solve the Schroedinger equation in quantum mechanics. After some algebra, the sought-after differential equation governing the evolution of the spectral density of a given TE mode, driven by an axially extended charge distribution propagating through a helically polarized wiggler is obtained:

$$\left(\frac{\omega^2}{c^2} - \frac{\chi'^2_{1q}}{a^2} + \partial_z^2 \right) \tilde{A}_{1q}(\omega,z) = \frac{\mu_0 q \beta_w J_2(\chi'_{1q} r_\perp/a) \exp\left[-\left(\omega \dfrac{\Delta z}{2\beta_\parallel c}\right)^2\right]}{\sqrt{2}\pi^{3/2} a^2 J_1^2(\chi'_{1q}) \left[1 - \left(\dfrac{1}{\chi'_{1q}}\right)^2\right]} \exp\left[i\left(\frac{\omega}{\beta_\parallel c} - k_w\right) z\right] \tag{38}$$

Note here that the wiggler helicity imposes a selection rule on the azimuthal wavenumber, further restricting the interaction to TE_{1q} modes. To obtain a clear picture of the physics involved in Eq. (38), we can introduce two different wavenumbers. First,

$$k_1(\omega) = \sqrt{\frac{\omega^2}{c^2} - \frac{\chi'^2_{1q}}{a^2}} \tag{39}$$

which corresponds to the propagation of the TE_{1q} mode in the cylindrical waveguide, and where we recognize the cutoff frequency associated with the mode, and

$$k_2(\omega) = \frac{\omega}{\beta_\parallel c} - k_w \tag{40}$$

which corresponds to the FEL Doppler-shifted beam mode as illustrated in Fig. 4. This mode involves the excitation of electrostatic space-charge waves on the electron beam and propagates at the axial beam velocity, as it is directly driven by the density modulation imposed on the beam by the external fields. With these definitions, Eq. (38) takes the considerably simpler form

$$d_z^2 f(z) + k_1^2 f(z) = C \exp(ik_2 z) \tag{41}$$

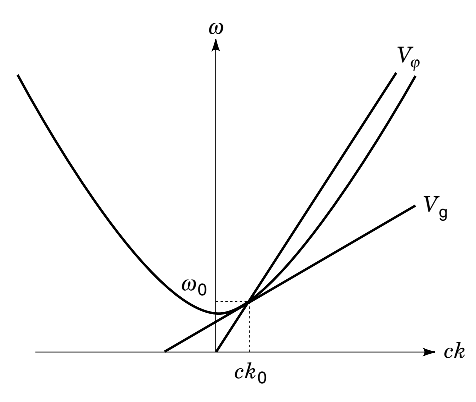

Figure 4. Dispersion diagram showing both the group and phase velocities.

which corresponds to a harmonic oscillator, with eigenfrequency k_1 (electromagnetic mode), driven harmonically at k_2 (beam mode). This system is driven resonantly when

$$k_1(\omega) = k_2(\omega) \tag{42}$$

which corresponds to the two roots $\omega = \omega^{\pm}$, where

$$\omega^{\pm} = \gamma_{\|}^2 \beta_{\|} k_w c \left[1 + \beta_{\|} \sqrt{1 - \left(\frac{\omega_c}{\gamma_{\|} \beta_{\|} k_w c} \right)^2} \right] \tag{43}$$

are the waveguide FEL Doppler upshifted and downshifted interaction frequencies. Here, ω_c is the cutoff frequency of the TE_{1q} mode under consideration. Taking the solution to Eq. (41) corresponding to forward propagation, and using the relation $\mathbf{E} = -\nabla\phi - \partial_t \mathbf{A}$, yields the Fourier transform of the electric field excited by the beam in the FEL interaction region

$$\begin{aligned} \tilde{\mathbf{E}}_{1q}(\omega, z) = {} & \frac{\sqrt{2} q \beta_w}{\pi^{3/2} \epsilon_0 a^2} g_{1q} \omega \exp\left[-\left(\frac{\omega\, \Delta z}{2\beta_{\|} c} \right)^2 \right] \\ & \times \frac{\sin[\Delta k(\omega)(z/2)]}{\Delta k(\omega)} \frac{\exp\{i[k_1(\omega) + k_2(\omega)](z/2)\}}{k_1(\omega) + k_2(\omega)} \end{aligned} \tag{44}$$

where we have defined the radial overlap integral of the bunch over the transverse eigenmode, g_{1q} (which is a geometrical factor indicating how efficiently the electron beam couples to a particular transverse mode, depending on its electromagnetic field distribution), and where the wavenumber detuning parameter has been introduced. The zeros of this parameter correspond to the FEL interaction frequencies given in Eq. (43).

The main features of this solution are the following. First, the amplitude of the electric field is proportional to the bunch charge and acceleration, which yields the usual quadratic scalings for the power spectrum. This is a general characteristic of coherent radiation processes, as illustrated in the N^2 scaling discussed in the Introduction. The next factor is the aforementioned overlap integral of the bunch transverse distribution with the TE mode. The exponential factor describes the degree of coherence of the radiation; its argument is a quadratic function of the bunch length to wavelength ratio. This means that for long wavelengths, the bunch essentially behaves like a point charge and radiates coherently, while at wavelengths shorter than the physical size of the electron bunch, the radiation is incoherent, as destructive interference between various parts of the bunch greatly diminish the resulting radiation intensity. The next factor, which appears in the form of a modified *sinc* ($\sin(x)/x$) function is the envelope of the radiation spectrum, containing the information that the interaction is maximized at the FEL resonant frequencies, where the detuning factor is zero and the *sinc* reaches its maximum value of unity. In the case of well separated Doppler upshifted and downshifted interaction frequencies, the denominator of the *sinc* function tends to zero linearly. By contrast, in the case of grazing, where the group velocity of the wave matches the axial bunch velocity, the denominator has a double singularity ($\omega^+ = \omega^-$), yielding a quadratic behavior and a maximized interaction bandwidth. Finally, the spectral phase information (coherence and chirp) is described by the argument of the complex exponential.

Therefore, the analysis of the dispersion characteristics of an electrodynamical system, using the Fourier-eigenmode expansion method described here, yields a number of important results pertaining to the spatial and temporal coherence of the radiation interacting with the system. The temporal characteristics of the wavepacket generated by the coherent synchrotron radiation process can also be analyzed by Fourier-transforming back into the time domain. This is now briefly sketched in the following paragraphs.

In general, it is not possible to derive an analytical expression for the time-dependent electromagnetic field in a complex electrodynamical structure. However, most of the physics of coherence and dispersion can be analyzed by using a Taylor expansion of the dispersion relation around a given frequency ω^*, which is often chosen to correspond with a resonant interaction frequency, such as those described in Eq. (43) for the FEL case. For the FEL, the wavenumber detuning is expanded around the resonant frequency as follows:

$$\begin{aligned} \Delta k(\omega - \omega^*) \cong {} & (\omega - \omega^*) \left(\frac{1}{\nu_g} - \frac{1}{\nu_{\|}} \right) - \frac{1}{2} \left(\frac{\omega - \omega^*}{\nu_g} \right)^2 \frac{d\nu_g}{d\omega} \\ & + \frac{1}{6} \left(\frac{\omega - \omega^*}{\nu_g} \right)^3 \left[2 \left(\frac{d\nu_g}{d\omega} \right)^2 - \nu_g \frac{d^2 \nu_g}{d\omega^2} \right] \end{aligned} \tag{45}$$

Here, the group velocity, GVD, and the cubic term are considered; higher-order terms can also be introduced to include other pulse distortions at large detuning parameters. Note that the linear term corresponds to slippage, which is the mismatch between the group velocity and the beam velocity. For a given type of interaction (slippage dominated, grazing, zero-dispersive grazing, etc.), corresponding to a minimal order of the Taylor expansion, the wavenumber detuning takes the general form

$$\Delta k(\omega - \omega^*) \cong a_n (\omega - \omega^*)^n \tag{46}$$

where

$$a_1 = \frac{1}{\nu_g} - \frac{1}{\nu_{\|}}$$

describes slippage,

$$a_2 = -\frac{1}{2} \frac{\nu_g'}{\nu_g^2}$$

corresponds to GVD, and

$$a_3 = -\frac{1}{6} \frac{\nu_g''}{\nu_g^2}$$

is the cubic term. At grazing, the first term is zero, and the interaction spectrum has a quadratic behavior near resonance, thus broadening the interaction bandwidth; other dispersive structures can yield even higher-order broadening, where the minimum order of the expansion becomes cubic, for example.

Using the Taylor expansion to Fourier-transform back into the time domain yields analytically tractable results, at least for low-order interactions. Slippage translates into linear pulse broadening, where the radiation pulse leads or lags behind the electron bunch, whereas at grazing, where slippage is eliminated, the temporal pulse broadening mechanism is GVD: the interaction bandwidth is large, and different frequency components of the pulse have different group velocities. The output pulse is also chirped by this mechanism (typically, the high frequencies propagate faster than the longer wavelengths, for a positive GVD medium). With negative GVD, pulse compression can be achieved. Finally, we note that very similar techniques are used at optical wavelength, including CPA, which is described in the section concerning optical coherence and quantum systems.

COHERENCE IN QUANTUM DEVICES

The other general type of electromagnetic source corresponds to quantum systems, where bound electrons can interact with the (external or virtual) radiation field. Three fundamental processes can occur in this situation: absorption, spontaneous emission, and stimulated emission. By comparison with the previously described, classical free-electron radiation sources, coherence now links and correlates the stimulated emission process, while spontaneous radiation is typically associated with incoherent radiation, where the statistical properties of the photon field correspond essentially to random noise fluctuations.

Two very important concepts are associated with quantum systems interacting electromagnetically: the quantization of the radiation field into the photon field, and Heisenberg's uncertainty principle, which sets a lower limit to the commutator of conjugate variables for both particles and fields. The first concept, introduced by Planck to describe the spectral characteristics of blackbody, or thermal equilibrium, radiation, was extended by Einstein to describe absorption and spontaneous radiation. As a result of this analysis, Einstein postulated the existence of a third type of radiation process: stimulated emission. One of the key features of stimulated radiation is its coherence: the phases of the incident and emitted photons are identical. The second concept introduces vacuum fluctuations: the electromagnetic field is described as an assembly of harmonic oscillators, with quantized energy levels corresponding to oscillation modes represented by photons. The energy spectrum associated with this model has the form $(n + 1/2)\hbar\omega$, where the lowest (vacuum) energy level has a nonzero value. The parameter $\hbar = 6.62\ 10^{-34}$ J · s is Planck's constant. Creation and annihilation operators are applied to describe the quantum dynamics of the photon number and are interpreted physically in terms of emission and absorption. Because of the nature of the quantum vacuum, which is now described in terms of virtual particles and satisfies the uncertainty principle, vacuum fluctuations can induce spontaneous transitions between different energy levels associated with the emission of incoherent spontaneous radiation.

Another important set of ideas in the early formulation of the quantum theory was concerned with the explanation of atomic spectral lines. The interaction of electromagnetic radiation with atoms became a very important research topic, and the discrete nature of atomic spectra yielded a strong indication that the energy levels in the atom must be quantized, in close connection with the quantization of electromagnetic energy in the form of photons. Bohr first explained the hydrogen spectrum in terms of quantization of the angular momentum, following de Broglie's argument that the particle-wave duality exhibited by the photon must have a counterpart for the electron and other subatomic particles. This early theoretical model of the hydrogen atom was subsequently shown to be a solution of Schroedinger's equation, which brings a formal basis to quantum mechanics.

The next development concerned the radiation theory of Dirac (10,11), where emission and absorption were described in terms of the interaction of the quantized electromagnetic field with atomic systems. It was also realized that a fully relativistic formulation of quantum electrodynamics was needed. Two types of problems immediately appeared: the point structure of the electron yielded an infinite electromagnetic mass, and the zero-point vacuum energy also resulted in severe divergences. The problem was solved by the introduction of modern QED by Feynman, Schwinger, Dyson and Tomonaga, who renormalized both the electron mass and charge to avoid the electromagnetic mass and vacuum polarization problems. The new roles of the electron and photon in QED, which also fully explained antiparticles, have important consequences for the concept of coherence in electrodynamics.

Absorption, Spontaneous Emission, and Stimulated Emission

Before considering superradiant processes and the quantum theory of optical coherence, it is interesting to briefly review the basic ideas behind the fluctuations in photon number. A detailed presentation is given in the classic monograph of Loudon (12). As mentioned earlier, the occurrence of absorption and emission processes causes the number of photons in each mode of the quantized radiation field to fluctuate. The ergodic theorm, often used in statistical mechanics, indicates that averaging a given system over time is equivalent to averaging over an ensemble of identical systems at a given time. In the case of photons, instead of time-averaging over a large cavity in space, one can average the photon number over the same field mode in large numbers of similar cavities. The fluctuations are then derived from the higher-order moments of the photon number probability distribution, with the result that $\Delta n = \sqrt{\langle n\rangle^2 + \langle n^2\rangle}$, where the brackets denote averaging. Such statistical fluctuations can be measured in photon-counting experiments.

The mechanism of emission and absorption of photons can first be described by means of a simple phenomenological theory proposed by Einstein. The postulates behind this simple model can actually be rigorously demonstrated using a quantum mechanical description of these interaction processes. In this model, the electromagnetic field is quantized in a cavity with fixed boundary conditions, and two-level atoms are considered. Photons can be emitted or absorbed if their frequency satisfies the condition $\hbar\omega_{12} = E_2 - E_1$, where E_1 is the ground state energy of the atoms, and E_2 is the energy of the excited state. The respective number of atoms, also called population, in each level is N_1 and N_2. Both the thermal energy density of the radiation and the contribution from an external probe beam must be considered; in this case, the total energy density in the cavity, at a frequency ω, is $W_t(\omega) + W_e(\omega)$. The photon absorption and emission probabilities are defined as follows. An excited atom has a transition rate A_{21} to spontaneously emit a photon and decay into the ground state. For an atom in the ground state, excitation is possible only if the atom absorbs a photon. The probability for this process, per unit time, is thus proportional to the photon energy density: B_{12} $W(\omega)$. Finally, as will be shown, a third process must be allowed to balance the equations describing the evolution of the population in the ground and excited states. This process, postulated by Einstein, is called stimulated emission and has the probability B_{21} $W(\omega)$.

For a sufficiently large total number of atoms, the rate equations governing the two levels are

$$\frac{dN_1}{dt} = -\frac{dN_2}{dt} = N_2A_{21} + [N_2B_{21} - N_1B_{12}]W(\omega) \tag{47}$$

To inspect the implications of this result more carefully, one can consider the simple case of thermal equilibrium. In any equilibrium configuration, the time derivatives are identically zero; in addition, for thermal equilibrium, there is no external energy density; therefore,

$$W_t(\omega) = \frac{A_{21}}{\left(\frac{N_1}{N_2}\right)B_{12} - B_{21}} \tag{48}$$

On the other hand, for thermal equilibrium, the populations obey Boltzmann's law, where

$$\frac{N_1}{N_2} = \exp\left(-\frac{E_1}{k_BT}\right)\exp\left(\frac{E_2}{k_BT}\right) = \exp\left(\frac{\hbar\omega_{12}}{k_BT}\right) \tag{49}$$

and an expression relating the energy density to the Einstein coefficients is obtained:

$$W_t(\omega_{12}) = \frac{A_{21}}{\exp\left(\frac{\hbar\omega_{12}}{k_BT}\right)B_{12} - B_{21}} \tag{50}$$

This expression can be directly compared with Planck's law for blackbody radiation. In the absence of stimulated emission, temperature independent balance cannot be achieved. Finally, this result must be independent of the equilibrium temperature, thus yielding the following relations for the coefficients:

$$B_{12} = B_{21} \tag{51}$$

$$\frac{\hbar\omega_{12}^3}{\pi^2c^3}B_{21} = A_{21} \tag{52}$$

This result shows that for an idealized, two-level atomic system, the transition rates can be expressed in terms of a single coefficient. Simple considerations also lead to the fact that, in thermal equilibrium, the emission rate stimulated by the blackbody photons is proportional to the spontaneous emission rate and the average photon number in the radiation modes at the transition frequency ω_{12}:

$$\frac{A_{21}}{B_{21}W_t(\omega_{12})} = \exp\left(\frac{\hbar\omega_{12}}{k_BT}\right) - 1 \tag{53}$$

For example, at room temperature, the wavelength scale of thermal radiation is of the order of 50 μm, and thermally stimulated emission will dominate at longer wavelengths. In the optical range, the spontaneous emission rate far exceeds the stimulated emission, thereby requiring pumping schemes for population inversion in lasers.

Quantum Theory of Optical Coherence

With the advent and rapid development of masers and lasers in the early 1960s, the concept of coherence that had been conventionally used in optics was found to be inadequate to completely describe the novel photon states produced by these sources. To provide a fuller discussion of coherence, a succession of correlation functions for the complex field strength was defined by Glauber (4), in his classic exposition of the quantum theory of optical coherence.

Chirped Pulse Amplification

Chirped pulse amplification (CPA) is a technique used to amplify ultrashort laser pulses (1 ps to 10 fs) to very high peak power levels (100 GW to 100 TW) through temporal expansion and recompression. With a time–bandwidth product defined by the laser pulse shape (i.e.: Gaussian $\Delta\omega\ \Delta\tau = 2$), short pulse length is directly correlated to large bandwidth. When such a pulse is incident on an optical diffraction grating, the various spectral components of the short pulse are spread spatially. By arranging a pair of optical gratings, the spatial separation is converted to an ordering of the spectral components in time. Under the proper set of circumstances, the chirped pulse output will have a duration of orders of magnitude (up to 100,000 demonstrated in the laboratory) larger than the original short pulse from the oscillator. The stretched pulse can be safely amplified without causing damage to the amplifier medium. Once amplified, the conjugate process to stretching is applied to recompress the now large amplitude laser pulse. This process relies directly on the spatial and temporal coherence of the incident ultrashort laser pulse and is a good example of a modern development in femtosecond optics.

Squeezed Optical States

Although the uncertainty principle imposes a lower bound on the commutator of conjugate variables, such as amplitude and phase for the quantized radiation field, the shape of the domain of phase space corresponding to a particular coherent state of light can be reshaped by means of nonlinear interactions. For example, the phase fluctuations can be smaller than those of the vacuum state. Of course, this is done at the expense of the conjugate variable. This is essentially the basic idea behind optical squeezing. Such modern developments in optics are also closely related with quantum nondemolition measurements, include those relying on Kerr-type nonlinearities, and with the concept of phase conjugation.

COHERENT EFFECTS IN LASER PRODUCED PLASMAS

Laser-produced plasmas are an important plasma source and a complex medium for the propagation of electromagnetic (EM) waves (14). They are important to applications such as inertial confinement fusion (ICF), study of relativistic plasma physics, acceleration of electrons to GeV energies (by means of laser EM fields or longitudinal plasma waves), and many other areas, including industrial applications. Since plasmas are composed of electrically charged particles, there is a strong coupling between the charged particles in the plasma and the EM fields of the laser. A number of processes can occur between the laser light and the plasma, such as absorption and coupling of the EM energy through a number of different processes. The plasma, produced by the laser pulse, is modified as the light pulse propagates through the plasma, modifying the electron density and temperature, the electron density gradient, and the overall geometry of the plasma. In turn, the plasma itself has a strong effect on the laser pulse, modifying its properties as it propagates, modifying the direction of propagation, its frequency, and its coherence.

Further complexities arise from the coupling of the EM wave to other modes inside the plasma (15). Since a plasma can support a family of longitudinal plasma waves, they can couple to the incident EM wave of the laser, producing secondary progeny waves, with one of the waves being an EM progeny wave with optical properties different from the incident "pump" EM wave. There are situations, on the other hand, where the properties of the laser field are modified on purpose. For applications such as ICF (16), the coherence of the laser beam is modified in an attempt to resolve problems associated with the coupling of the laser to the ICF plasmas.

We will consider the following three issues associated with the propagation of an EM wave of high intensity through a plasma: harmonic generation near the critical density; decay of the incident laser light through parametric processes; and the purposely modified coherence of a laser beam. These three cases address situations where the laser light dramatically changes its frequency (generation of harmonics), has a strong modification to its frequency (loss of energy to a local longitudinal model of the plasma), and the reduction of spatial or temporal coherence of the light to minimize detrimental effects.

Harmonics of the laser light can be generated at the critical density of a laser-produced plasma, where electrons are forced to oscillate by the electric field of the laser, in and out of a region of plasma of varying density. Critical density is the density at which the frequency of the laser light equals the frequency of the plasma, a point at which total reflection of the light occurs. The EM field of the laser causes a nonsinusoidal oscillation of the electrons, yielding the generation of higher harmonics. The process responsible for this is the ponderomotive force associated with the resonant absorption of light. Resonance absorption is a linear process by which a light wave is partially absorbed by conversion into an electrostatic wave at the critical surface (17). A light wave incident onto an inhomogeneous plasma is reflected at the classical turning point determined by $n_e = n_{cr} \cos^2\theta$, where θ is the angle of incidence. For a p-polarized wave, the electric field of the light wave is in the plane formed by its propagation vector $\underline{k}$ and $\underline{\nabla} n_e$. At the turning point, the local electric field points in the direction of $\underline{\nabla} n_e$. Some of this field tunnels to the critical surface region, where it resonantly drives an electron plasma oscillation. Part of the light wave energy is thus converted into an electrostatic wave, which heats the plasma electrons as it damps. This process does not occur for s-polarized light. The electric field of the light wave is then perpendicular to both $\underline{k}$ and $\underline{\nabla} n_e$ and so does not drive charge density fluctuations.

A self-consistent steepening of the density profile is an essential feature of the resonant absorption of intense light waves. In an expanding plasma, any pressure exerted at any point will locally modify the density profile, which produces a localized steepening. One example of this is the momentum deposition of the incident light reflecting at its critical density. A more complex situation arises if p-polarized laser light is incident at an oblique angle with respect to the plasma density gradient. In this case, the steepening of the density profile is produced both by the pressure of the reflected obliquely incident light and by the pressure of a resonantly generated electrostatic field near the critical density. When electrons oscillating in the resonantly-driven field move into regions of higher and lower electron density, the electron oscillation becomes nonsinusoidal. Harmonic components are superimposed on their oscillations and similarly on the radiated EM wave. The number of harmonics will be a function of the intensity of the laser light and the steepness of the electron density gradient. This process has produced harmonics to high orders (>50) when driven by long wavelength lasers, such as CO_2 (18). The interest in this area has been reopened with the new, high-power, short-pulse lasers (19).

Strong modification to the frequency spectrum of the laser light can be induced by the decay into secondary EM as a byproduct of a decay associated with a parametric process (14,15). Laser plasma coupling can be strongly influenced by the excitation of plasma waves either by mode conversion near the critical density as discussed above (resonance absorption) or by a variety of instabilities. These instabilities can be most simply represented as the resonant coupling of the incident laser light into two other waves. If we neglect magnetic fields, these progeny waves are simply high-frequency electron plasma waves (Langmuir), low-frequency ion acoustic waves, and scattered electromagnetic waves. The stimulated Brillouin scattering (SBS) and the stimulated Raman (SRS) instabilities have been studied extensively during the past twenty years, both theoretically and experimentally. Stimulated Brillouin scattering consists of the decay of the incident EM wave (ω_o, $\boldsymbol{k}_o$) into a scattered EM wave (ω_{SBS}, $\boldsymbol{k}_{SBS}$) and an IAW (ω_{IAW}, $\boldsymbol{k}_{IAW}$), where ω and $\boldsymbol{k}$ are the respective frequency and wavevector for each wave. Similarly, stimulated Raman scattering consists of the decay of the incident EM wave into a scattered EM wave (ω_{SRS}, $\boldsymbol{k}_{SRS}$) and an IAW (ω_{EPW}, $\boldsymbol{k}_{EPW}$). For example, in the stimulated Raman instability, the laser light can decay into a scattered light wave and an electron plasma wave. In the Brillouin instability, the two progeny waves are a scattered light wave and a low frequency ion acoustic wave. A decay into an electron plasma wave plus an ion acoustic wave (or a purely growing ion fluctuation) is also possible, and this process can occur near the critical density. In addition to the above processes, the laser light can produce density modulations which lead to either self-focusing or filamentation. All these instabilities have the consequence of modifying the incident laser light. The EM waves so generated are shifted in frequency, proportional to the energy taken by the local plasma mode, either the electron plasma wave or ion acoustic wave. For all these processes, the coherence length of the interaction beam is an important factor of the coupling. As the light propagates through the plasma, its wavenumber varies as a function of the local plasma conditions. This limits the region of interaction in which the three waves are resonant (14,15).

An interesting situation of coherence in laser-produced plasmas is when, on purpose, one needs to reduce it as much as possible. The coherence of a laser beam can be detrimental to an application such as ICF. Inertial confinement fusion targets require extremely smooth laser beams to prevent hydrodynamic instabilities that can destroy the target symmetry during implosion. Some method to control the laser intensity and to reduce the spatial variations in beam intensity is needed, normally referred to as "beam smoothing" (20). Beam smoothing may also suppress the growth of laser plasma instabilities, such as SBS, SRS, and filamentation. Although reductions have not been clearly demonstrated (21), spatial smoothing is an important element in the study of parametric instabilities (22–24).

Two different approaches to smooth beam have been developed: spatial smoothing by breaking up the focal spot illumination into spatially fine-scale structures; and temporal smoothing by causing that structure to change rapidly with time, forming a temporally changing pattern. The spatial approach was first implemented using a random phase plate (RPP). An RPP is a transparent substrate with a random pattern of phase elements that introduce a phase shift of π in the incident light (25). The far-field intensity distribution consists of an overall envelope determined by an individual phase plate element. Within this envelope, there is a fine-scale speckle structure due to the interference between different phase element contributions whose dimensions are determined by the *f*/ number of the focusing optics. This produces spatial smoothing of the laser beam, creating a well-characterized laser focal spot which is nearly independent of the particular aberrations of the initial laser beam. Temporal smoothing, on the other hand, requires converting laser temporal incoherence (bandwidth) into temporally varying spatial incoherence, causing the target spot intensity distribution to change in time (26). Since the relative phases of these beamlets will change every coherence time, this causes the speckle pattern on target to change in time.

BIBLIOGRAPHY

1. C. Davisson and L. H. Germer, Diffraction of electrons by a crystal of nickel, *Phys. Rev.,* **30**: 705–740, 1927.
2. M. R. Andrews et al., Observation of interference between two Bose condensates, *Science,* **275**: 637–641, 1997.
3. S. Weinberg, *The Quantum Theory of Fields,* Cambridge: Cambridge University Press, 1995.
4. R. J. Glauber, The quantum theory of optical coherence, *Phys. Rev.,* **130**: 2529–2539, 1963.
5. L. Mandel and E. Wolf, *Optical Coherence and Quantum Optics,* Cambridge: Cambridge University Press, 1995.
6. W. Pauli, *Theory of Relativity,* New York: Dover Publications, Inc., 1958.
7. J. D. Jackson, *Classical Electrodynamics,* New York: Wiley, 1975.
8. P. A. M. Dirac, Classical theory of radiating electrons, *Proc. R. Soc. London Ser.,* **A167**: 148–169, 1938.
9. C. W. Roberson and P. Sprangle, A review of free electron lasers, *Phys. Fluids,* **B1**: 3–42, 1989.
10. J. Schwinger (ed.), *Selected Papers on Quantum Electrodynamics,* New York: Dover Publications, 1958.
11. W. Heitler, *The Quantum Theory of Radiation,* Oxford: Oxford University Press, 1954.
12. R. Loudon, *The Quantum Theory of Light,* Oxford: Oxford University Press, 1983.
13. R. H. Dicke, Coherence in spontaneous radiation processes, *Phys. Rev.,* **93**: 99–110, 1954.
14. W. L. Kruer, *The Physics of Laser Plasma Interactions,* Redwood City, CA: Addison-Wesley, 1988.
15. H. A. Baldis, E. M. Campbell, and W. L. Kruer, Laser-plasma interactions, in *Physics of Laser Plasma,* A. Rubenchik and W. Witkowski (eds.), Amsterdam: North-Holland, 1991, pp. 361–434.
16. W. L. Lindl, R. L. McCrory, and E. M. Campbell, Progress towards ignition and burn propagation in inertial confinement fusion, *Phys. Today,* **45**: 32, 1992.
17. V. L. Ginzburg, *The Propagation of Electromagnetic Waves in Plasmas,* Oxford: Pergamon, 1970.
18. R. L. Carman, C. K. Rhodes, and R. F. Benjamin, *Phys. Rev,* A **24**: 2649, 1981.
19. J. S. Wark et al., Measurements of the hole boring velocity from Doppler shifted harmonic emission from solid targets, *Phys. Plasmas,* **3**: 3242, 1996.
20. H. T. Powell, S. N. Dixit, and M. A. Henesian, Beam smoothing capability on the Nova laser, *ICF Quarterly Report,* **1**: 28, Lawrence Livermore National Laboratory, Livermore, CA, UCRL-LR-105821-91-1, 1990.
21. J. D. Moody et al., Beam smoothing effects on the stimulated Brillouin scattering (SBS) instability in Nova exploding foil plasmas, *Phys. Plasmas,* **2**: 4285, 1995.
22. V. T. Tikhonchuk, C. Labaune, and H. Baldis, Modeling of a stimulated Brillouin scattering experiment with statistical distribution of speckles, *Phys. Plasmas,* **3**: 3777, 1996.
23. C. Labaune et al., Interplay between ion acoustic waves and electron plasma waves associated with stimulated Brillouin and Raman scattering, *Phys. Plasmas,* **4**: 423, 1997.
24. H. A. Baldis et al., Resonant seeding of stimulated Brillouin scattering by crossing laser beams, *Phys. Rev. Lett.,* **77**: 2957, 1996.
25. Y. Kato et al., Random phasing of high-power lasers for uniform target acceleration and plasma instability suppression, *Phys. Rev. Lett.,* **53**: 1057, 1984.
26. R. H. Lehmberg and S. P. Obenschain, Use of induced spatial incoherence for uniform illumination of laser fusion targets, *Opt. Commun.,* **46**: 27, 1983.

F. V. Hartemann
H. A. Baldis
Institute for Laser Science and Applications of LLNL
N. C. Luhmann, Jr.
University of California at Davis
Gregory P. Le Sage
Lawrence Livermore National Laboratory

COIL INSULATION TESTING. See Insulation testing.

COLLECTORS, SOLAR. See Solar heating.

COLOR ANLAYSIS OF IMAGES. See Image color analysis.